Growth of gold nanorods nucleated by HgTe nanoparticle seeds on various surfaces

Siyka I. Shopova[a], Charles W. Blackledge[a], Nicholas F. Materer[b], and A. T. Rosenberger[*a]
[a]Department of Physics, Oklahoma State University, 145 Physical Sciences, Stillwater, OK USA 74078-3072;
[b]Department of Chemistry, Oklahoma State University, 107 Physical Sciences I, Stillwater, OK USA 74078-3071

Keywords: Gold nanorods, nucleation, HgTe nanoparticles, semiconductor-metal nanocomposites, microresonators

ABSTRACT

We describe the synthesis of gold nanorods (NRs) nucleated by HgTe nanoparticles (NPs) of average size 3 nm in diameter. Growth of ~200 nm by ~50 nm NRs on various surfaces is achieved by using an intermediary polyelectrolyte layer. A poly(dimethyldiallylammonium) chloride (PDDA) monolayer on the surface attracts the thioglycolic acid (TGA) capped HgTe NPs and assists in one-dimensional gold growth. Rod morphology is observed for approximately one third of the resulting features. Confirmation of Au deposition is obtained with x-ray photoelectron spectroscopy and optical absorption measurements that show an increase in the Au plasmon band with time spent in gold growth solution. Au NRs were grown directly on the surface of high quality factor (Q) optical resonators (microspheres and microcylinders). Although the coating procedure reduces the Q of the resonators, whispering gallery modes are sustained. This seeding technique, amenable to many different surfaces, may result in semiconductor-metal nanocomposites with novel electronic and optical properties.

1. INTRODUCTION

Solution-phase colloidal preparation of gold nanorods (NRs) provides a facile way of fabricating materials with tunable optical properties. The size and shape of these metallic NRs together with the dielectric permittivity of the surrounding medium, tune the plasmon resonance of the Au NRs from the visible to the near infrared (500 nm to 1500 nm).[1, 2] These particles have enormous extinction coefficients that depend on their composition[3] and the ratio of length to width, or aspect ratio (AR).[4, 5] Unlike photoemission from organic dyes or quantum dots, the Au NR plasmons do not bleach or blink.[6]

Au NRs are yielded when Au nanoparticles (NPs) with variable capping agents are added to an aqueous solution containing anionic gold(I) dichloride ($AuCl_2^-$), ascorbic acid, and cetyltrimethylammonium bromide (CTAB). At room temperature the reaction does not proceed at an appreciable rate until NP seeds are added because of the free energy barrier of forming a new interface. The mechanisms for Au NR nucleation and growth are currently under intense investigation.[7, 8]

To utilize these particles in chemical and biological sensors, and other optical devices, immobilization is required. Two different approaches have been used: (1) immobilizing Au nanorods from solution by using one or a few intermediate layers on the substrate surface,[9, 10] and (2) direct growth on the surface. In the second approach gold NP seeds have been attached to the surface prior to immersing the substrate in the growth solution.[11-14]

The contribution of this work is using semiconducting HgTe NP seeds capped with thioglycolic acid (TGA) to nucleate gold NRs with morphology comparable to previous work.[12, 13] There are some advantages of using HgTe NPs to initiate Au growth. This method is a simple way to coat surfaces with different electrical and optical properties with a submonolayer of semiconducting NPs using an intermediary polyelectrolyte layer,[15] thus initiating growth of rods directly on the surfaces. The PDDA layer serves not only to attach seeds and NRs to the surface but also assists in the one-dimensional growth process. We achieve growth of Au NRs directly on curved surfaces, for example a silica microsphere that is a high quality optical resonator.[16] Finally, the use of semiconducting HgTe NP seeds, which have electronic states in the same spectral region (500 nm to 2000 nm)[17, 18] as the longitudinal mode of the metallic Au NR plasmon, offers a possibility of synthesizing composite nanomaterials with unique optical and electrical properties.

[*] atr@okstate.edu

Plasmonics: Metallic Nanostructures and Their Optical Properties III, edited by Mark I. Stockman,
Proceedings of SPIE Vol. 5927 (SPIE, Bellingham, WA, 2005) · 0277-786X/05/$15 · doi: 10.1117/12.617601

2. SYNTHESIS

The three-step procedure for growing Au NRs from HgTe NPs bound to surfaces is depicted in Fig. 1A-C. In the first step, the surface is dipped in an aqueous solution of polydimethyldiallyammonium (PDDA) chloride for ~30 minutes (Fig. 1A). This polyelectrolyte coating is applied to glass, mica, fused silica, and silicon surfaces. After washing with deionized water, the substrate is dipped in an aqueous solution of TGA-capped HgTe NPs for ~5 s to deposit a fraction of a monolayer of HgTe particles (Fig. 1B).[16] The concentration of seeds on the surface was kept low, approximately 20-40 NPs/μm^2, to enable the growth of well separated Au rods. The negatively charged carboxylate group of the HgTe NP capping agent is electrostatically bound to the quaternary amines of PDDA, and the interaction is robust enough to withstand washing with water. Next, the substrates are immersed in a gold growth solution of 1.3×10^{-4} m (molal) tetrachlorauric acid ($HAuCl_4$ - 99%, Sigma-Aldrich), 8.0×10^{-3} m cetyltrimethylammonium bromide (99%, Sigma-Aldrich), and 1.9×10^{-4} m ascorbic acid (99%, Sigma-Aldrich).

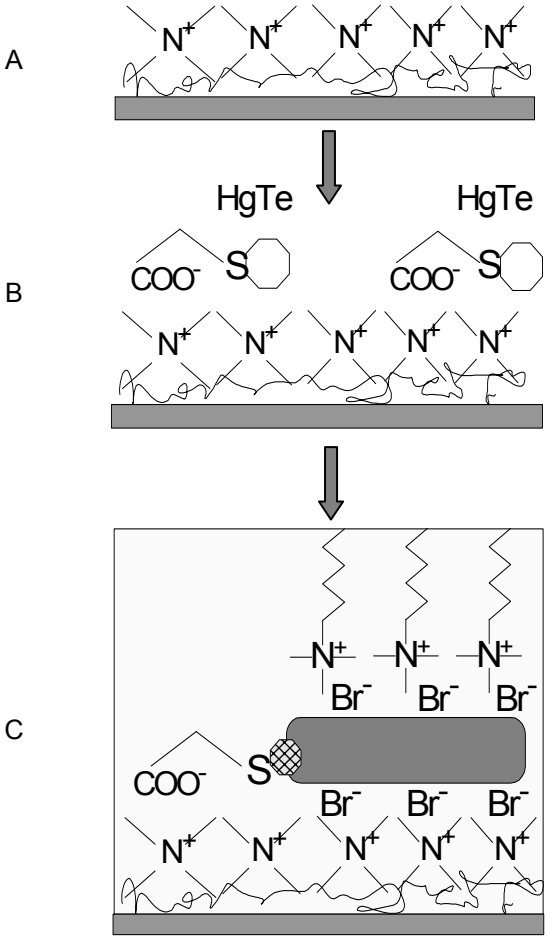

Figure 1. (A) The substrate is coated with a monolayer of PDDA, washed with deionized water and dried. (B) A submonolayer of HgTe NPs, capped with TGA, is formed on top of the PDDA layer. (C) The sample is immersed in Au growth solution, where one-dimensional growth is assisted by the presence of CTAB and the PDDA layer.

The ascorbic acid reduces $AuCl_4^-$ to $AuCl_2^-$ and other Au^+ species before the substrate is dipped into the solution. Further reduction to solid Au^0 is enabled by heterogeneous nucleation induced by the HgTe NP seeds. Originally transparent samples begin to turn pink in approximately 5 minutes, indicating Au deposition on the surface. Fig. 1C

depicts one possible outcome, in which the HgTe seed induces rod growth such that it remains at one end of the NR. It is also possible that Au growth occurs from both sides of HgTe crystal. High resolution transmission electron microscopy (HRTEM) is expected to give more information about this process.

Both HgTe and Au form face centered cubic structures, but the lattice constants are 0.65 nm and 0.41 nm, respectively. This implies that the elastic strain and defect density in the first few layers of Au atoms to deposit is greater when HgTe seeds are used and suggests that anisotropic growth could start even earlier, compared to the synthesis that uses Au seeds. When Au NPs are used as seeds, multifaceted particles up to a size of approximately 20 nm form before anisotropic rod growth begins.[19] At this size, rod growth begins because the crystal is large enough for preferential binding of CTAB to (110) or (100) crystal faces.[20] This asymmetrically hinders growth, allowing faster growth along directions free of CTAB. The positively charged quaternary amines of CTA^+ are attracted to the Br^- layer that is adsorbed to the lateral faces of the NRs. A bilayer of CTAB forms that shields the aliphatic tail of the surfactant from the aqueous environment (not shown in Fig. 1C).[2, 8, 21, 22] The PDDA derivatized surfaces may play a similar or competitive role to CTAB in the growth mechanism because the quaternary amines of PDDA are also electrostatically attracted to the Br^- layer. This interaction attaches the NR to the surface without an intermediary CTAB layer. Selected TEM images of resulting particles are given in Fig. 2.

3. CHARACTERIZATION

For characterization of the samples, transmission electron microscopy (TEM) is performed with a JEOL (JEM 100 CX II) at 100 kV, scanning electron microscopy (SEM) with a JEOL (JXM 6400) at 30 kV, atomic rorce microscopy (AFM) with a Digital Instruments Nanoscope IIIa, visible-NIR absorption spectroscopy with a Varian Cary 5, energy dispersive X-ray (EDX) with an EVEX Analytical System, and x-ray photoelectron spectroscopy (XPS) measurements are performed with a Mg K_α source and PHI double-pass cylindrical mirror analyzer with a pass energy of 50 eV.

3.1 Imaging

The particle shapes and sizes are similar to reports of Au NRs nucleated on surfaces using Au NPs.[12] From TEM (Fig. 2) and SEM (Fig. 3) images, NR's lengths are 235 ± 90 nm, widths are 50 ± 20 nm, and resulting aspect ratios are 4.7 ± 2.3. AFM measurements include any adsorbed PDDA and tip-size convolution, and yield lengths of 153 ± 43 nm, widths of 70 ± 11 nm, and heights of 36 ± 6 nm, with aspect ratios (length/height) of 4.3 ± 1.3.

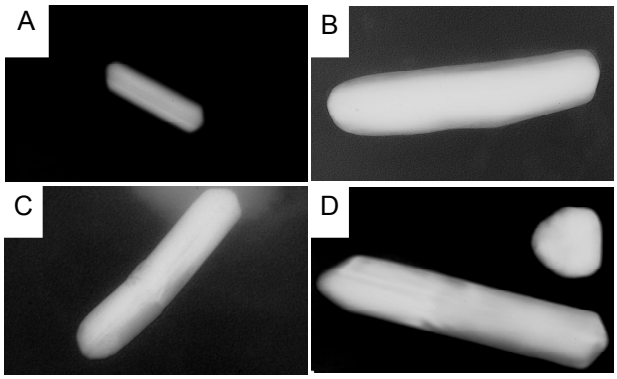

Figure 2. TEM images of Au rods nucleated with HgTe NPs on TEM formvar-coated grids. Rod size (A) 128.5 × 35.7 nm; (B) 270 × 62.9 nm; (C) 262 × 55.2 nm; (D) 333 × 66 nm.

Approximately one-third of the features in all the electron microscopy and AFM images that result from nucleation of Au by surface-bound HgTe NPs are rods with aspect ratios between 2 and 7. This yield is similar to that of Au NRs nucleated from surface bound Au NPs.[11-14] Figure 3A is an SEM image of a sample made with a low density of HgTe NPs bound to the surface of a silica microsphere, Fig. 3B is an SEM image of a sample grown on mica, and Fig. 4 and Fig. 5 show AFM results on glass and silicon surfaces, respectively.

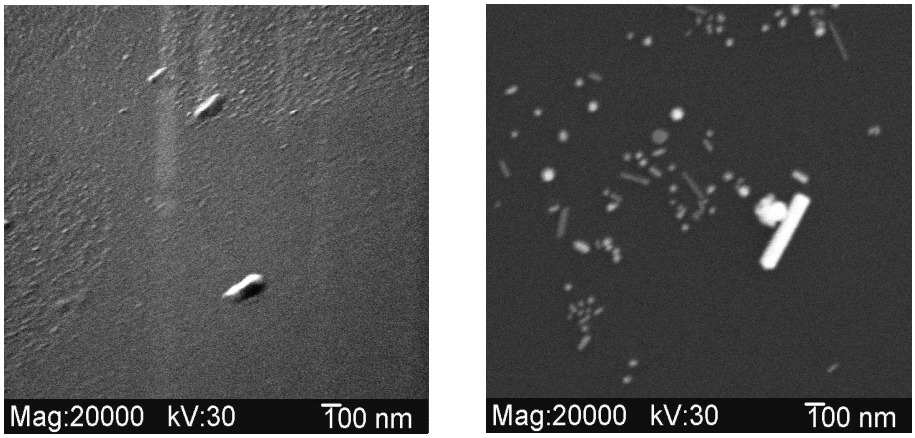

Figure 3. (A) SEM image of Au rods grown on the surface of a fused silica microsphere of diameter 450 μm. (B) SEM of rods grown on a mica surface.

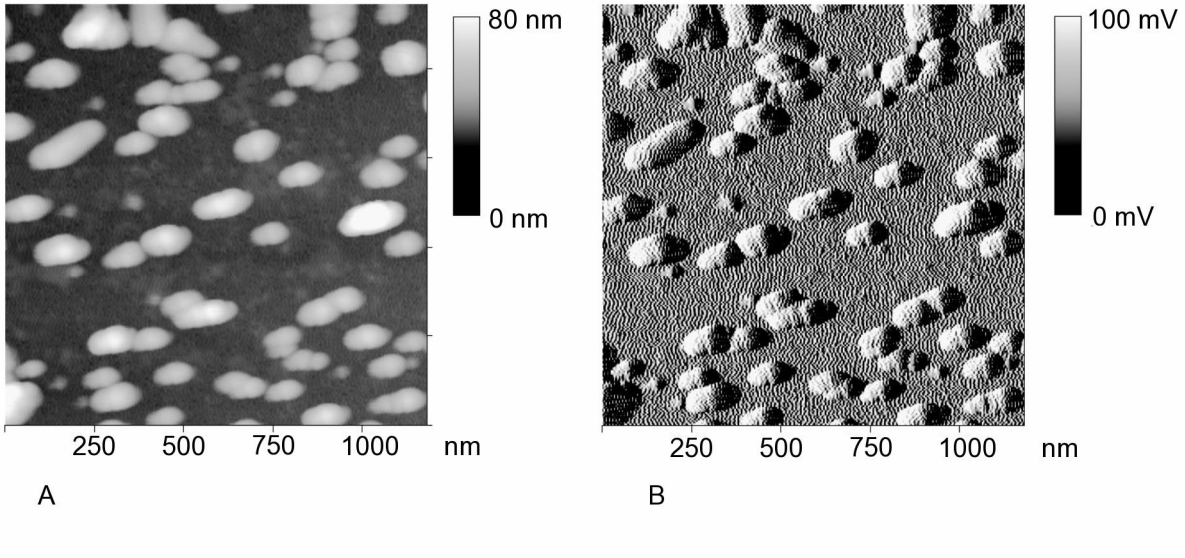

Figure 4. AFM height (A) and amplitude (B) images of gold rods grown on a microscope glass slide. The scan size is 1.18 μm and the maximum height on the brightness scale is 80 nm.

.

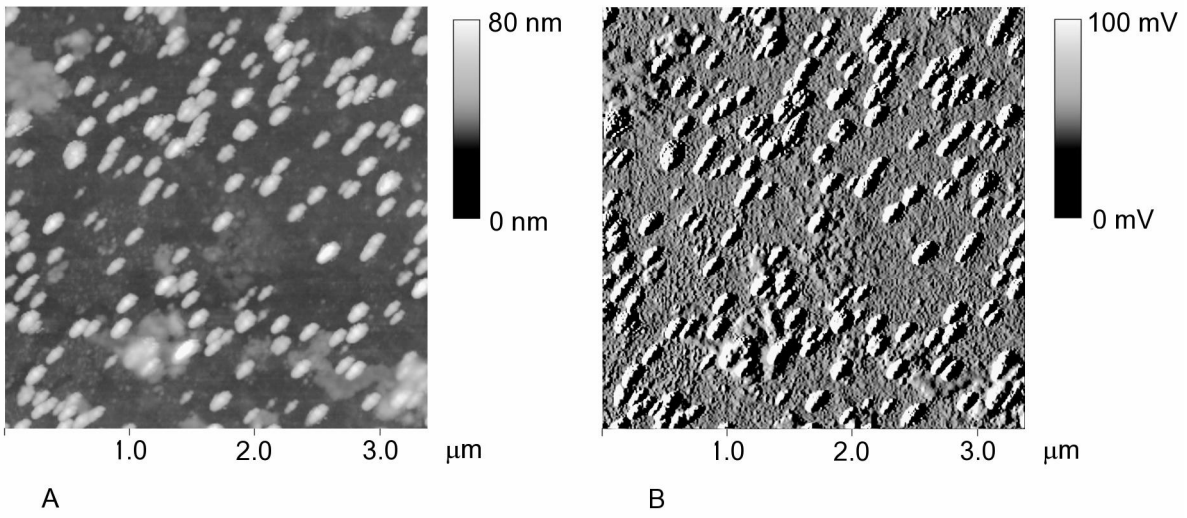

Figure 5. AFM height (A) and amplitude (B) images of gold rods grown on silicon. The scan size is 3.33 μm and the maximum height on the brightness scale is 80 nm.

The PDDA adsorbed to the surface of the NRs contributes to the AFM size measurements but not to those of electron microscopy, in which contrast is due to the relatively high electron density of the metal rods compared to their surroundings. Also, AFM results in an overestimation of topographical feature size due to the well known tip-shape convolution.

3.2 Spectroscopy

Different types of spectroscopy are used to confirm the presence of gold, mercury, and telluride on the surfaces. The presence of gold is supported by EDX, XPS, and absorption spectroscopy. Another important question is the presence of HgTe on the surface after immersion in the gold growth solution. XPS is performed to obtain information about the resulting states of the Hg and Te components after the growth procedure.

3.2.1 EDX

Energy dispersive X-ray analysis on the coated surfaces shows a Au peak. The problem with this technique is that the peak of EDX for Hg overlaps the Au peak. The resolution capabilities of the instrument are not sufficient to resolve the two peaks. A backscattered image (Fig. 6) of the area on the surface from which EDX was taken shows bright objects, also indicative of metal surfaces.

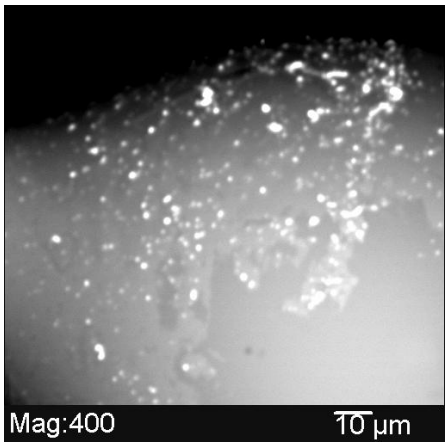

Figure 6. Backscattered image of gold grown on the surface of a 380 μm fused silica microsphere.

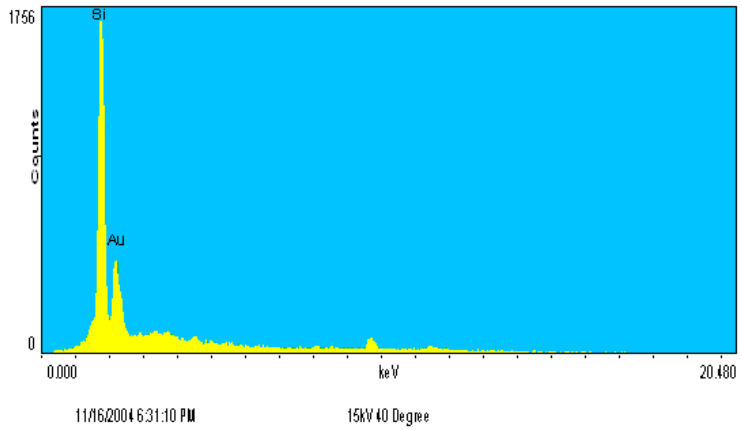

Figure 7. EDX taken of the surface of the fused silica microsphere shown in Figure 6. Peak identification results: Si 1.763 keV, Au 2.230 keV.

3.2.2 XPS

Additional evidence that the Au NR are nucleated by HgTe NPs is provided by XPS. Figure 8A shows the increase in the spin-orbit Au 4f doublet at binding energies of 83 and 87 eV as a function of reaction time for a sample prepared on a glass substrate. The increasing signal is correlated to an increasing surface concentration of Au due to the growth of the Au NRs. The Hg 4f spin-orbit doublet at 104 and 100 eV (Fig. 8B) is unfortunately masked by a large Si 2p signal at 103 eV due to the glass substrate. Figure 8C clearly shows that the Te 3d5/2 signal remains even after the sample is exposed for 45 min to the Au growth solution. The position and width of the Te 3d5/2 peak (575.5-580 eV, Fig. 8C) does not change significantly during the growth. This suggests that the local environment around the Te does not change significantly and that the HgTe NP remains intact during the Au NR growth. The result implies also that the Te does not become buried within the growing Au NR. In addition, the position of this peak suggests that a significant fraction of the Te is in an oxidized form, even before Au deposition.[23] Due to the large surface/volume ratio and exposure to the atmosphere, the 3-nm diameter HgTe NPs are likely to have a significant amount of surface oxide present.

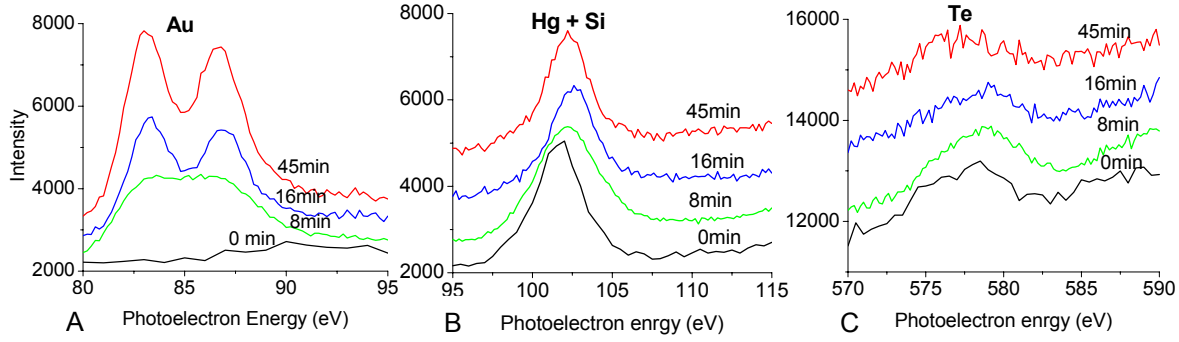

Figure 8. XPS of samples grown on glass substrates for different times in Au growth solution. The bottom line is a sample of HgTe NPs adsorbed to the surface. (This sample was not immersed in Au growth solution.) (A) The Au 4f spin-orbit doublet at 83 and 87 eV; (B) overlapping Hg 4f (from the nucleation particle) and Si 2p (from the substrate) around 100 eV; (C) the Te 3d5/2 (from the nucleation particle) at 575 - 580 eV.

3.2.3 Absorption Spectroscopy

3.2.3.1 Experimental

Figure 9 shows the time evolution of the absorption spectra of samples grown on glass. The samples were removed from the Au growth solution at different times, rinsed with water, and dried in air. The results are similar to those of Au NRs grown on surfaces using Au NPs as seeds.[13] The bottom line on Fig. 9A is a spectrum of the control sample. This surface was coated with PDDA but without deposited HgTe NPs. The spectrum confirms that Au growth does not occur without seeds.

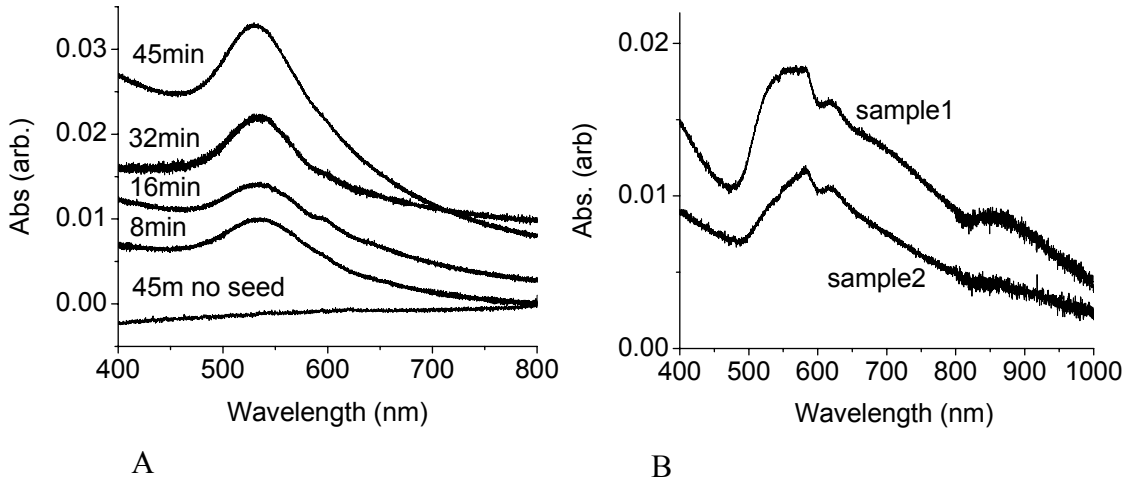

Figure 9. (A) Visible-NIR spectra of Au growth results on glass substrates for different times in Au growth solution. The bottom line is a control sample without HgTe NP nucleation seeds kept in growth solution for 45 minutes. (B) Vis-NIR spectra of Au growth on glass surfaces immersed in different batches of growth solution for 30 min.

The main contributions of the peaks in Fig. 9A are from spheres with relatively large diameters. The rods' longitudinal plasmon peak at 600 nm appears in the spectrum of the 16 min. sample and adds to the overall broadening of the other curves. AFM of the samples used in Fig. 9A shows rods with low ARs between 2 and 3 and a significant amount of spheres with diameters about half of the long axes of the rods. Comparison of the experimental result of Fig. 9A with calculated spectra indicate that roughly one sixth of the resulting particles are rods. Spectra of samples 1 and 2 in Fig. 9B have more fractional contribution from the rods' longitudinal plasmon. The ratio between rods and spheres in these samples is close to 1:3. The main difference in the preparation of samples on Figure 9A and 9B is the use of different purity of CTAB and also different seeds. Higher yield of rods was obtained using CTAB of 99% purity.

3.2.3.2 Calculated

Theoretical extinction coefficients are calculated for spherical Au particles and randomly oriented Au NRs modeled as ellipsoids.[24, 25] Published values for n and k (the real and imaginary components of the index of refraction)[26] for bulk gold and an interpolation method are used for calculating the dielectric permittivity of gold as function of the wavelength. A Gaussian distribution of aspect ratios is assumed. Contributions of nanospheres of different number and volume fractions are also taken into account. Figure 10 represents calculations for two different values of dielectric permittivity of the surrounding medium: (A) air, $\varepsilon_m = 1$; and (B) liquid, $\varepsilon_m = 2$. The spheres are chosen to have diameters equal to half of the average size rod's long axis.

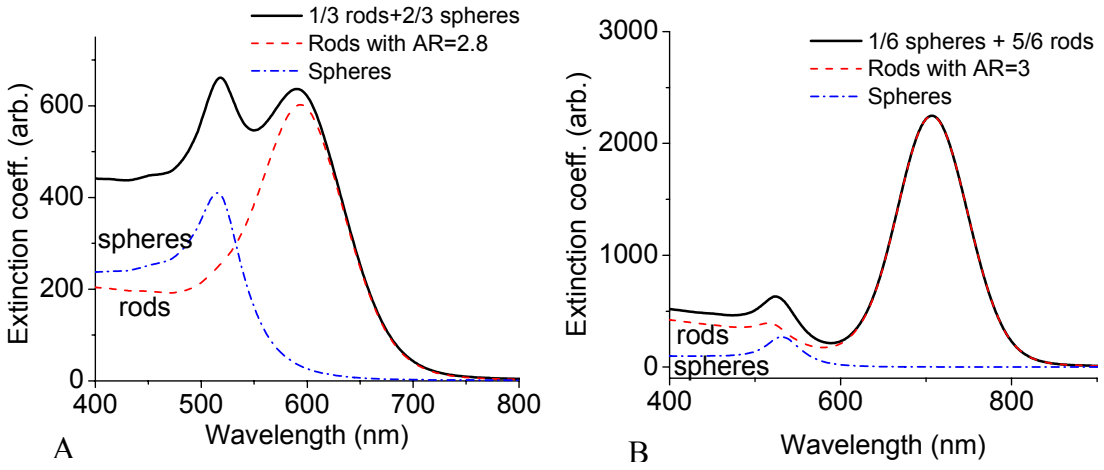

Figure 10. Calculated values of the extinction coefficients for (A) a mixture of 1/3 rods of AR = 2.8 ± 1 and 2/3 spheres in air with $\varepsilon_m = 1$, and (B) a mixture of 5/6 rods of AR = 3.0 ± 0.3 and 1/6 spheres in solution with $\varepsilon_m = 2$.

The calculations show that the magnitude of the transverse mode is much smaller and shows less change in λ_{max} when the aspect ratio is varied, compared to the longitudinal mode. The contribution of the spheres, even a small fraction (Fig. 10B), is not negligible and has to be taken into account. In air, the longitudinal mode of rods overlaps the transverse mode if the AR is less than 3 and also overlaps with the spheres' plasmon mode and may appear as a slightly split mode or as one broad mode. These calculations present a way to estimate the fractions of spheres versus rods in a colloidal solution and on surfaces, provided the density is low.

4. MICRORESONATORS

Nanorods are successfully grown on the surface of high quality optical resonators. The initial quality factor of the resonators before coating the surface is typically more than 10^8. After growth, the quality factor is reduced to the order of 10^5-10^6, if the density of nanorods is kept below 10 per μm^2 (only a fraction of a monolayer). Figure 3A shows SEM images of the surface of a microsphere which had a quality factor of 10^5 after Au growth.

After preparing the resonator in this way, light of 830 nm from a cw, tunable Ti:Sapphire laser was coupled to it using a tapered fiber. The schematic is given in Fig. 11. The frequency scan shows whispering gallery modes of a microsphere with Au NRs grown on the surface.

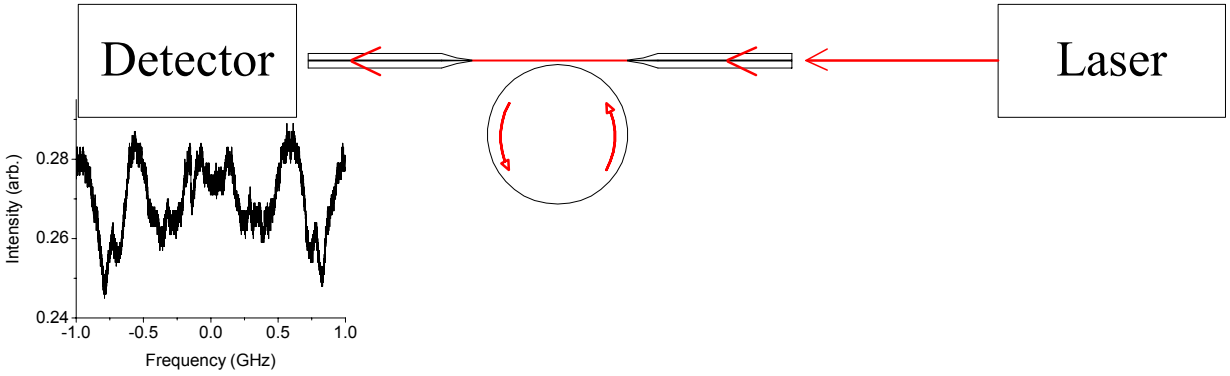

Figure 11. Coupling light from a tunable laser source to the microresonator. As the laser is tuned in frequency and the resonant frequency of the resonator is reached, light gets trapped, by total internal reflection, into the resonator and a drop in power is observed on the detector, as indicated in the frequency trace of detected power.

Light inside the microresonator is making many roundtrips (depending on the quality factor) until it dies out, thus interacting with the nanoparticles on the surface of the resonator. If the light of excitation has a frequency in the range of the plasmonic mode, an enhancement of luminescence and perhaps lasing is expected. Gigantic increases of the Raman signal of metal aggregates on the surface of a microresonator have been observed.[27] Noncoated microsphere resonators have been used as chemical sensors[28] for gases and liquids. Introducing gold nanorods on the surface of these resonators should enable surface-enhanced Raman to provide additional chemical detection sensitivity.

5. CONCLUSIONS

In conclusion, the synthesis of Au NRs using HgTe NPs as nucleation seeds is demonstrated. The method provides a simple way to permanently attach gold nanorods on surfaces with different electrical and optical properties. Further work is underway to determine the nanometer scale composition distribution, optical properties, and to build simple optoelectronic circuits that help characterize the NR/NP composites, and explore avenues of device fabrication. Simple circuits made from purely metallic Au NRs have already been fabricated and characterized.[29] For the composite nanomaterial, the proximity of the HgTe NP to the gold NR, and the overlap of excitonic states with the Au plasmon resonance, is expected to strongly modulate the photoemissive properties such as lifetime and quantum yield, dephasing time, electron and hole mobility, and the bleaching and blinking rates.

ACKNOWLEDGMENTS

This work was supported by the National Science Foundation under Awards No. ECS-0115442, No. ECS-0329924, and No. EPS-0132534. The authors thank Dr. Nicholas A. Kotov for supplying the HgTe NPs, and Dr. Bret N. Flanders and Dr. James P. Wicksted for laboratory space and loan of some equipment.

REFERENCES

1. Y. Yu, S. Chang, C. Lee, and C. Wang, "Gold nanorods: Electrochemical synthesis and optical properties," J. Phys. Chem. B, **101**, 6661-6664, 1997.
2. A. Gole, and C. Murphy, "Seed-mediated synthesis of gold nanorods: Role of the size and nature of the seed," Chem. Mater., **16**, 3633-3640, 2004.
3. S. Link, Z. Wang, and M. El-Sayed, "Alloy formation of gold-silver nanoparticles and the dependence of the plasmon absorption on their composition," J. Phys. Chem. B, **103**, 3529-3533, 1999.
4. S. Link, and M. El-Sayed, "Optical properties and ultrafast dynamics of metallic nanocrystals," Annu. Rev. Phys. Chem., **54**, 331-366, 2003.
5. C.-H. Chou, C.-D. Chen, and C. R. C. Wang, "Highly efficient, wavelength-tunable, gold nanoparticle based optothermal nanoconvertors," J. Phys. Chem. B, 2005.
6. C. Sonnichsen, and A. Alivisatos, "Gold nanorods as novel nonbleaching plasmon-based orientation sensors for polarized single-particle microscopy," Nano Lett., **5**, 301-304, 2005.
7. C. J. Murphy, T. K. Sau, A. M. Gole, C. J. Orendorff, J. Gao, L. Gou, S. E. Hunyadi, and T. Li, "Anisotropic metal nanoparticles: Synthesis, assembly, and optical applications," J. Phys. Chem. B, ASAP, 2005.
8. J. Perez-Juste, L. Liz-Marzan, S. Carnie, D. Chan, and P. Mulvaney, "Electric-field-directed growth of gold nanorods in aqueous surfactant solutions," Adv. Funct. Mater., **14**, 571-579, 2004.
9. A. Gole, C. Orendorff, and C. Murphy, "Immobilization of gold nanorods onto acid-terminated self-assembled monolayers via electrostatic interactions," Langmuir, **20**, 7117-7122, 2004.
10. Y. Niidome, H. Takahashi, S. Urakawa, K. Nishioka, and S. Yamada, "Immobilization of gold nanorods on the glass substrate by the electrostatic interactions for localized plasmon sensing," Chem. Lett., **33**, 454-455, 2004.
11. H. Liao, and J. Hafner, "Monitoring gold nanorod synthesis on surfaces," J. Phys. Chem. B, **108**, 19276-19280, 2004.
12. N. Taub, O. Krichevski, and G. Markovich, "Growth of gold nanorods on surfaces," J. Phys. Chem. B, **107**, 11579-11582, 2003.
13. Z. Wei, A. Mieszawska, and F. Zamborini, "Synthesis and manipulation of high aspect ratio gold nanorods grown directly on surfaces," Langmuir, **20**, 4322-4326, 2004.

14. A. J. Mieszawska, and F. Zamborini, "Gold nanorods grown directly on surfaces from microscale patterns of gold seeds," Chem. Mater., **17,** 3415-3420, 2005.
15. Z. Tang, Y. Wang, and N. Kotov, "Semiconductor nanoparticles on solid substrates: Film structure, intermolecular interactions, and polyelectrolyte effects," Langmuir, **18**, 7035-7040, 2002.
16. S. I. Shopova, G. Farca, A. T. Rosenberger, W. M. S. Wickramanayake, and N. A. Kotov, "Microsphere whispering-gallery-mode laser using HgTe quantum dots," Appl. Phys. Lett., **85**, 6101-6103, 2004.
17. D. Koktysh, N. Gaponik, M. Reufer, J. Crewett, U. Scherf, A. Eychmuller, J. Lupton, A. Rogach, and J. Feldmann, "Near-infrared electroluminescence from HgTe nanocrystals," ChemPhysChem, **5**, 1435-1438, 2004.
18. A. Rogach, D. Koktysh, M. Harrison, and N. Kotov, "Layer-by-layer assembled films of hgte nanocrystals with strong infrared emission," Chem. Mater., **12**, 1526-1528, 2000.
19. C. Johnson, E. Dujardin, S. Davis, C. Murphy, and S. Mann, "Growth and form of gold nanorods prepared by seed-mediated, surfactant-directed synthesis," J. Mater. Chem., **12**, 1765-1770, 2002.
20. Z. Wei, and F. Zamborini, "Directly monitoring the growth of gold nanoparticle seeds into gold nanorods," Langmuir, **20**, 11301-11304, 2004.
21. B. Nikoobakht, and M. El-Sayed, "Preparation and growth mechanism of gold nanorods (NRs) using seed-mediated growth method," Chem. Mater., **15**, 1957-1962, 2003.
22. T. Sau, and C. Murphy, "Seeded high yield synthesis of short Au nanorods in aqueous solution," Langmuir, **20**, 6414-6420, 2004.
23. C. D. Wagner, A. V. Naumkin, A. Kraut-Vass, J. W. Allison, C. J. Powell, and J. R. Rumble Jr, "X-ray photoelectron database," *National Institute of Standards and Technology*, http://srdata.nist.gov/xps/
24. R. Gans, "Form of ultramicroscopic particles of silver," Ann. Physik, **47**, 270-284, 1915.
25. G. C. Papavassiliou, "Optical properties of small inorganic and organic metal particles," Prog. Solid State Chem., **12**, 185-271, 1980.
26. P. B. Johnson, and R. W. Christy, "Optical constants of the noble metals," Phys. Rev. B, **6**, 4370-4379, 1972.
27. W.-T. Kim, V. P. Safonov, V. P. Drachev, V. A. Podolskiy, V. M. Shalaev, and R. L. Armstrong, "Fractal-Microcavity Composites: Giant Optical Responses," *Optical properties of nanostructured random media*, V. M. Shalaev, **82**, 149-167, Springer, Berlin, 2002.
28. G. Farca, S. I. Shopova, and A. T. Rosenberger, "Intracavity chemical absorption sensing using microresonator whispering-gallery modes," *17th International Conference on Optical Fibre Sensors*, Proceedings of SPIE, M. Voet, R. Willsch, W. Ecke, J. Jones and B. Culshaw, **5855**, 427-430, 2005.
29. B. Ozturk, C. Blackledge, and B. Flanders, "Structural and transport properties of reproducible interconnects dielectrophoretically assembled from gold nanorods," Appl. Phys. Lett., Submitted, 2005.